Indian J Pure Appl Math (2026) 57:1362–1378
https://doi.org/10.1007/s13226-024-00683-4

ORIGINAL RESEARCH

Effect of slippage on a translational motion of two interacting non-concentric spheres squeezed by couple stress fluid

Shreen El-Sapa · **Noura S. Alsedais**

Received: 26 August 2023 / Accepted: 20 August 2024 / Published online: 23 October 2024

Abstract This investigation shows the couple stress fluid filled the space between the two non-concentric spheres under the effect of slippage. Therefore, this work is innovative due to the application of the velocity slip conditions to the surfaces of the spheres. In addition, the two spheres are translating axially at various linear speeds. The solution is obtained semi-analytically at low Reynolds numbers utilizing the superposition with the numerical collocation approach. This paper discusses the hydrodynamic drag force exerted by the fluid on the internal particle. Consequently, it is found that all the results agreed with the corresponding numerical analysis in the traditional viscous liquids and the traveling of two eccentric rigid spheres with no slippage.

Keywords Slippage condition · Translation motion · Drag · Couple stress fluids · Collocation method

1 Introduction

Due to the limitations of traditional nonpolar fluids in accurately describing the behavior of fluid flow containing suspended particles, there has been a significant focus on the theory of polar fluids in recent years. The analysis of these fluids is important in a variety of industrial processes, including but not limited to crude oil extraction from petroleum products, fluid heating, electrostatic precipitation, liquid crystal solidification, cooling processes of metal plates in a bath, the use of exotic lubricants, and the study of colloidal and suspension solutions. Stokes' [1,2] couple stress fluid, which includes polar effects, is one example of a fluid with distinct properties. The introduction of a length-dependent effect, which is not typically observed in nonpolar fluids, is the primary factor contributing to couple stresses. The Poiseuille, Couette, and generalized Couette flows of an incompressible couple stress fluid through parallel plates with slip boundary conditions have all been solved analytically by Devakar et al. [3]. Gajjela et al. [4] has performed an analysis of the numerical solutions for the generation of entropy in a porous-lined annulus between two rotating cylinders subject to a radial magnetic field. Podila et al. [5] investigated the oscillating motion of an incompressible Couple Stress fluid through a permeable sphere. Rabia Naz et al. [6] studied the analytical solutions of the incompressible and unsteady movement of a couple stress liquid flow modeled with a power law fractional differential operator that fills the partial space $y > 0$ over a smooth (solid) plate covering the *xz*-plane.

Communicated by N. M. Bujurke.

S. El-Sapa (✉)
Department of Mathematics and Computer Science, Faculty of Science, Damanhour University, Damanhour, Egypt
E-mail: s_elsapa82@sci.dmu.edu.eg

N. S. Alsedais
Department of Mathematical Sciences, College of Science, Princess Nourah bint Abdulrahman University, 11671 Riyadh, Saudi Arabia
E-mail: nsalsudais@pnu.edu.sa

Overall, when fluid flows past rigid boundaries, the no-slip boundary condition is employed. However, many applications have observed and investigated liquid slips on a solid surface, it has recently been recognized that some fluids, including additive fluids and polymerics, can stick to and slide along rigid boundaries. "Navier introduced a more general boundary condition—that the fluid velocity component tangential to the solid surface, relative to the solid surface, is proportional to the shear stress on the fluid–solid interface" to describe the slip characteristics of fluid on the solid surface. Results from molecular dynamics simulations of Newtonian liquids under shear were presented by Thompson and Troia [7], and they show that there is a general nonlinear relationship between the magnitude of slip and the local shear rate at the surface of solid material. Ashmawy [8] studied the dynamics of a rigid slip sphere immersed in a couple stress fluids with a linear slip boundary condition on the surface. He found that the normalized drag force decreases as the couple stress viscosity parameter increases. Through an inclined peristaltic asymmetric channel, Akram et al. [9] mathematically explained the significance of partial slip-on double-diffusive convection on magneto-Carreau nanofluid. El-Sapa and Almoneef [10] investigated the effect of slip and spin slip on the surface of a porous couple stress fluid-immersed solid sphere. They observed that the normalized drag force increases due to the slip and spin slip effects.

Furthermore, many different numerical algorithms have been used to solve ordinary differential equations or partial differential equations with high-order accuracy. Among these methods is the collocation method, which has been widely used to solve problems in a variety of fields, including computational fluid dynamics, magnetohydrodynamics, and optics. The collection method's basic idea is that the velocity field is defined by an ordered sequence of basic solutions appropriate to the constant orthogonal surface that will be presented. and the solution series is truncated, and the boundary conditions are not applied exactly to the entire body, but only at a few carefully selected points known as collocation points. Gluckman [11] was the first to develop a new method for dealing with slow viscous motion past finite assemblages of random-shaped particles. Chang and Keh [12] used the boundary collocation method to study the slow motion of a spherical fluid or solid particle with a slip-flow surface in a viscous fluid perpendicular to two parallel planes. Sherief et al. [13] used the collocation technique to investigate the slow motion of an oscillating spherical particle in a viscous fluid located within a semi-infinite viscous fluid bounded by an impermeable plane. The spectral collocation method was applied by Sun et al. [14] for studying coupled radiative and thermal conductivity in concentric cylinders.

The objective of this study is to give semi-analytical solutions for the axisymmetric movements of a solid sphere that translates into a non-concentric hollow filled with stress fluids under the influence of slippage surfaces. Due to this, the boundary collocation procedure is utilized in the equation system. Additionally, given various values of the relevant parameters such as the slippage, the separation, the size ratio, the couple stress, and the angular velocity ratios, then the normalized torque acting on the interior solid sphere can be calculated. Across all parameters, the results showed good convergence and are displayed visually and calculated tabularly.

2 Mathematical formulation

By the notion of a low Reynolds number, without the presence of body forces and body couples, the field constraints controlling the steady motion of an incompressible couple stress liquid are dictated by [2]:

$$\mathrm{u}_{i,i} = 0, \tag{1}$$

$$\mu\, \mathrm{u}_{i,jj} - \eta\, u_{i,jjkk} - p_{,i} = 0\,. \tag{2}$$

Here, the constant μ is the fluid viscosity, η is the viscosity of 1st couple stress, u_i is the velocity of the fluid, and is the fluid pressure. If the relation (2) tends to the classical equation of Navier–Stokes. The tensor forms of t_{ij} and m_{ij} are [2]

$$\tau_{ij} = -p\,\delta_{ij} + 2\mu\, d_{ij} - \tfrac{1}{2}\, e_{ijk}\, m_{sk,s}\,, \tag{3}$$

$$m_{ij} = m\delta_{ij} + 4(\eta\,\omega_{j,i} + \eta'\,\omega_{i,j})\,, \tag{4}$$

where η' is 2nd couple stress, m is a tensor trace of couple stress, the two tenors are Kronecker delta, e_{ijk} is alternating tensor, d_{ij} is deformation rate tensor, and $\vec{\omega}$ is vorticity vector, the two last concepts are formed as:

$$d_{ij} = \frac{1}{2}(u_{i,j} + u_{j,i})\,, \quad \omega_i = \frac{1}{2} e_{ijk}\, u_{k,j}\,. \tag{5}$$

The enforced boundary constraints may be used to derive the scalar quantity that was mentioned in relation (4). Additionally, one may explicitly define it as [1] by using the second relation of (4) and the concept of (5):

$$m = \frac{1}{3} m_{ii} \,. \tag{6}$$

The physical constants in the fundamental equations (3) and (4), as well as the equation for movement (2), are presumed to adhere to the following constraints in [2]:

$$\mu \geq 0, \ \ \eta \geq 0, \ \ \eta \geq \eta' \,. \tag{7}$$

Furthermore, suppose that the surface of the sphere is subject to the following circumstances., $r = a$:

(a) Slippage restriction

$$\beta \ (u - U \ \sin\theta) = t_{r\theta} \,, \tag{8}$$

Where β is the slippage parameter changing its values from zero to infinity. This coefficient is only related to the type of fluid and the material's surface. Furthermore, the perfect slip situation becomes possible when the slip coefficient disappears, and the traditional no-slip case may be inferred as a specific instance in this study when the slip parameter approaches infinity. The slippage condition of the boundary has recently been used to solve several viscous fluids [9–12] and micropolar fluids [26,27] issues.

(b) The prevailing condition is the absence of couple stresses [2]

$$m_{ij} \, n_i = 0 \quad \text{on} \quad r = a, \tag{9}$$

where n_i is the unit normal to the surface of the solid sphere. Stokes [1] has suggested the boundary conditioning equation (9). Only in this situation can mechanical interactions at the borders produce a force distribution, according to physical theory.

3 Axisymmetric solution to the problem

In an incompressible couple stress liquid, allow us to assume that the translational motion of a sphere with radius a travels symmetry about its axis. The spherical systemic process is set up at the sphere's center; the field functions are independent of ϕ . In addition, the vorticity and velocity vectors are shown by:

$$\vec{u} = (u_r(r,\theta), \ \ u_\theta(r,\theta), \ \ 0) \,, \tag{10}$$

$$\vec{\omega} = \big(0, \ 0, \ \omega_\phi(r,\theta)\big) \tag{11}$$

In view of the equation of continuity (2.1), one can write the velocity components in terms of the stream function ψ as

$$\left.\begin{aligned} u_r &= \frac{-1}{r^2 \sin\theta} \frac{\partial\psi}{\partial\theta}, \\ u_\theta &= \frac{1}{r \sin\theta} \frac{\partial\psi}{\partial r} \end{aligned}\right\} . \tag{12}$$

Substitute Eq. (10) into the momentum equation (2) by eliminating the pressure, the subsequent p.d.e is obtained as:

$$E^4 \left[E^2 - \kappa^2 \right] \psi \ \ = 0, \tag{13}$$

where the material constant $1/\kappa = \sqrt{\eta / a^2 \mu}$, is taken into consideration as a polarity indicator for the couple stress fluids approach, and the Stokesian indicator of axial motion is:

$$E^2 = \frac{\partial^2}{\partial r^2} + \frac{1 - \zeta^2}{r^2} \frac{\partial^2}{\partial \zeta^2}, \qquad \zeta = \cos\theta \,. \tag{14}$$

Furthermore, the tangential stress is calculated by El-Sapa and Almoneef [7] as:

$$\tau_{r\theta} = 2\mu \, e_{r\theta} - \frac{1}{2} \left[\frac{\partial m_{r\phi}}{\partial r} + \frac{(2m_{r\phi} + m_{\phi r})}{r} + \frac{\cot\theta}{r} (m_{\theta\phi} + m_{\phi\theta}) + \frac{1}{r} \frac{\partial m_{\theta\phi}}{\partial\theta} \right] . \tag{15}$$

We obtain the following regular axisymmetric stress and couple stresses by using the tensor relation (4):

$$E_{r\theta} = \frac{1}{2}\left[\frac{1}{r}\frac{\partial u_r}{\partial \theta} - \frac{u_\theta}{r} + \frac{\partial u_\theta}{\partial r}\right] \tag{16a}$$

$$m_{r\phi} = 4\eta\frac{\partial \omega_\phi}{\partial r} - 4\eta'\frac{1}{r}\omega_\phi \tag{16b}$$

$$m_{\phi r} = -4\eta\frac{1}{r}\omega_\phi + 4\eta'\frac{\partial \omega_\phi}{\partial r} \tag{16c}$$

$$m_{\theta\phi} = 4\frac{1}{r}\left[\eta\frac{\partial \omega_\phi}{\partial \theta} - \eta'\cot\theta\omega_\phi\right] \tag{16d}$$

$$m_{\phi\theta} = 4\frac{1}{r}\left[-\eta\cot\theta\omega_\phi + \eta'\frac{\partial \omega_\phi}{\partial \theta}\right] \tag{16e}$$

The tangential stress can be modified by using Eq. (15) into (14) as:

$$\tau_{r\theta} = \mu\left[\frac{1}{r}\frac{\partial u_r}{\partial \theta} - \frac{u_\theta}{r} + \frac{\partial u_\theta}{\partial r}\right] - 2\eta\left[\frac{\partial^2 \omega_\phi}{\partial r^2} + \frac{2}{r}\frac{\partial \omega_\phi}{\partial r} + \frac{1}{r^2}\left(\frac{\partial^2}{\partial \theta^2} + \cot\theta\frac{\partial}{\partial \theta} - \csc^2\theta\right)\omega_\phi\right]. \tag{17}$$

The differential equation (12) has the following generalized solution:

$$\begin{aligned}\psi = \sum_{n=2}^{\infty}\Big[&A_n r^{-n+1} + B_n r^{-n+3} + C_n\sqrt{r}\,K_{n-\frac{1}{2}}(\kappa r)\\ &+D_n r^n + E_n r^{n+2} + F_n\sqrt{r}\,I_{n-\frac{1}{2}}(\kappa r)\Big]\Im_n(\zeta),\end{aligned} \tag{18}$$

where the two functions $K_n(.)$ and $I_n(.)$the first and second types of modified Bessel functions of order n, respectively. Also, $G_n(.)$ denotes the Gegenbauer polynomial of the first kind of order n and degree $-1/2$.

By using (16) and (18), we reach

$$\begin{aligned}u_r = &-\sum_{n=2}^{\infty}\left(A_n r^{-n-1} + B_n r^{-n+1} + C_n r^{-3/2}K_{n-\frac{1}{2}}(\kappa r)\right)P_{n-1}(\zeta)\\ &-\sum_{n=2}^{\infty}\left(D_n r^{n-2} + E_n r^n + F_n r^{-3/2}I_{n-\frac{1}{2}}(\kappa r)\right)P_{n-1}(\zeta),\end{aligned} \tag{19}$$

where $P_n(.)$ is denoting Legendre polynomial of order n.

$$\begin{aligned}u_\theta = &\sum_{n=2}^{\infty}\left[(1-n)A_n r^{-n-1} + (3-n)B_n r^{-n+1} + C_n\, r^{-3/2}\left(n\,K_{n-\frac{1}{2}}(\kappa r) - \kappa r K_{n+\frac{1}{2}}(\kappa r)\right)\right]\frac{\Im_n(\zeta)}{\sqrt{1-\zeta^2}}\\ &+\sum_{n=2}^{\infty}\left[n\,D_n r^{n-2} + (n+2)E_n r^n + F_n\, r^{-3/2}\left(\kappa r I_{n+\frac{1}{2}}(\kappa r) + n\,I_{n-\frac{1}{2}}(\kappa r)\right)\right]\frac{\Im_n(\zeta)}{\sqrt{1-\zeta^2}}\end{aligned} \tag{20}$$

Equation (18) is applied to Eqs. (14) and (15), and the resulting vorticity components are as follows:

$$\begin{aligned}\omega_\phi = &\frac{1}{2}\sum_{n=2}^{\infty}\left[2(3-2n)B_n r^{-n} + C_n\kappa^2 r^{-1/2}K_{n-\frac{1}{2}}(\kappa r)\right]\frac{\Im_n(\zeta)}{\sqrt{1-\zeta^2}}\\ &+\frac{1}{2}\sum_{n=2}^{\infty}\left[2(2n+1)E_n r^{n-1} + F_n\kappa^2 r^{-1/2}I_{n-\frac{1}{2}}(\kappa r)\right]\frac{\Im_n(\zeta)}{\sqrt{1-\zeta^2}},\end{aligned} \tag{21}$$

Applying Eqs. (19) and (20) to Eq. (17) yields the stresses and couple stresses:

$$\begin{aligned}e_{r\theta} = \sum_{n=2}^{\infty}\Big[&(n^2-1)A_n r^{-n-1} + n(n-2)B_n r^{-n}\\ &+\frac{1}{2}C_n r^{-5/2}\left((\kappa^2 r^2 + 2n^2 - 4n)K_{n-\frac{1}{2}}(\kappa r) + 2\kappa r K_{n+\frac{1}{2}}(\kappa r)\right)\Big]\frac{\Im_n(\zeta)}{\sqrt{1-\zeta^2}}\end{aligned}$$

$$+ \sum_{n=2}^{\infty}\Big[n(n-2)D_n r^{n-3} + (n^2-1)E_n r^{n-1}$$
$$+ \frac{1}{2}F_n\ r^{-5/2}\left((\kappa^2 r^2 + 2n^2 - 4n)I_{n-\frac{1}{2}}(\kappa r) - 2\kappa r I_{n+\frac{1}{2}}(\kappa r)\right)\Big]\frac{\Im_n(\zeta)}{\sqrt{1-\zeta^2}} \tag{22}$$

$$m_{r\phi} = \sum_{n=2}^{\infty}\Big[4n(2n-3)(\eta+\eta')B_n r^{-n-1}$$
$$+2C_n\,\kappa^2\, r^{-3/2}\left((\eta(n-1)-\eta')K_{n-\frac{1}{2}}(\kappa\, r) - \kappa\, r\eta K_{n+\frac{1}{2}}(\kappa\, r)\right)\Big]\frac{\Im_n(\zeta)}{\sqrt{1-\zeta^2}}$$
$$+\sum_{n=2}^{\infty}\Big[4(2n+1)(\eta(n-1)-\eta')E_n\, r^{n-2}$$
$$+2F_n\,\kappa^2\, r^{-3/2}\left((\eta(n-1)-\eta')I_{n-\frac{1}{2}}(\kappa\, r) + \kappa\, r\eta I_{n+\frac{1}{2}}(\kappa\, r)\right)\Big]\frac{\Im_n(\zeta)}{\sqrt{1-\zeta^2}} \tag{23}$$

$$m_{\phi r} = \sum_{n=2}^{\infty}\Big[4n(2n-3)(\eta+\eta')B_n r^{-n-1}$$
$$+2C_n\,\kappa^2\, r^{-3/2}\left((\eta'(n-1)-\eta)K_{n-\frac{1}{2}}(\kappa\, r) - \kappa\, r\eta' K_{n+\frac{1}{2}}(\kappa\, r)\right)\Big]\frac{\Im_n(\zeta)}{\sqrt{1-\zeta^2}}$$
$$+\sum_{n=2}^{\infty}\Big[4(2n+1)(\eta(n-1)-\eta')E_n\, r^{n-2}$$
$$+2F_n\,\kappa^2\, r^{-3/2}\left((\eta'(n-1)-\eta)I_{n-\frac{1}{2}}(\kappa\, r) + \kappa\, r\eta' I_{n+\frac{1}{2}}(\kappa\, r)\right)\Big]\frac{\Im_n(\zeta)}{\sqrt{1-\zeta^2}} \tag{24}$$

$$m_{\theta\phi} = 2\sum_{n=2}^{\infty}\left[2(3-2n)B_n r^{-n-1} + C_n\,\kappa^2\, r^{-3/2}K_{n-\frac{1}{2}}(\kappa\, r)\right]\frac{\left(\eta(n-1)-\eta'\right)\Im_n(\zeta) - (n-2)\eta\Im_{n-1}(\zeta)}{\sqrt{1-\zeta^2}}$$
$$+2\sum_{n=2}^{\infty}\left[2(2n+1)E_n\, r^{n-2} + F_n\,\kappa^2\, r^{-3/2}I_{n-\frac{1}{2}}(\kappa\, r)\right]\frac{\left(\eta(n-1)-\eta'\right)\Im_n(\zeta) - (n-2)\eta\Im_{n-1}(\zeta)}{\sqrt{1-\zeta^2}} \tag{25}$$

$$m_{\phi\theta} = 2\sum_{n=2}^{\infty}\left[2(3-2n)B_n r^{-n-1} + C_n\,\kappa^2\, r^{-3/2}K_{n-\frac{1}{2}}(\kappa\, r)\right]\frac{\left(\eta'(n-1)-\eta\right)\Im_n(\zeta) - (n-2)\eta'\Im_{n-1}(\zeta)}{\sqrt{1-\zeta^2}}$$
$$+2\sum_{n=2}^{\infty}\left[2(2n+1)E_n\, r^{n-2} + F_n\,\kappa^2\, r^{-3/2}I_{n-\frac{1}{2}}(\kappa\, r)\right]\frac{\left(\eta'(n-1)-\eta\right)\Im_n(\zeta) - (n-2)\eta'\Im_{n-1}(\zeta)}{\sqrt{1-\zeta^2}} \tag{26}$$

Employing the obtained Eqs. (19), (20) and (22)–(26) into (17), we get:

$$\tau_{r\theta} = \sum_{n=2}^{\infty}\Big[2\mu(n^2-1)A_n\, r^{-n-2} + 2\mu n(n-2)B_n r^{-n}$$
$$+\ C_n\, r^{-5/2}\left(\left(\mu(\kappa^2 r^2 + 2n^2 - 4n) - \eta\kappa^4 r^2\right)K_{n-\frac{1}{2}}(\kappa r) + 2\mu\kappa r K_{n+\frac{1}{2}}(\kappa r)\right)\Big]\frac{\Im_n(\zeta)}{\sqrt{1-\zeta^2}}$$
$$+\sum_{n=2}^{\infty}\Big[2\mu n(n-2)D_n r^{n-3} + 2\mu(n^2-1)E_n r^{n-1}$$
$$+\ F_n\ r^{-5/2}\left(\left(\mu(\kappa^2 r^2 + 2n^2 - 4n) - \eta\kappa^4 r^2\right)I_{n-\frac{1}{2}}(\kappa r) - 2\mu\kappa r I_{n+\frac{1}{2}}(\kappa r)\right)\Big]\frac{\Im_n(\zeta)}{\sqrt{1-\zeta^2}} \tag{27}$$

The resultant drag force acting on the axisymmetric particle is found to be acting along the axis of symmetry and has a magnitude of [8]:

$$F_z = 4\pi \mu B_2. \tag{28}$$

Ramkissoon [20] has studied the steady flow of an incompressible couple stress fluid past a rigid sphere of radius. He concluded that the spherical particle is subject to the following drag force:

$$F_\infty = -6\mu U a^3 \left\{1 + \frac{\alpha}{\kappa a}\right\}, \quad \alpha = \frac{2 + \eta'/\eta}{\kappa a + 2 + \eta'/\eta}\,, \tag{29}$$

3.1 Hydrodynamic interaction of translating two eccentric spheres filled with a couple stress fluid.

For this simulation, it is assumed the annulus between the two non-concentric spheres of radii $a_j,\ j = 1, 2$ s filled with a constant density of couple stress liquid. Therefore, the sphere and the spherical cavity are translating along the connecting line of its centers with distinct speeds U_1 ad U_2, respectively and at a distance h from their centers, as shown in Fig. 1. Consider that $u_r^{(1)},\ u_\theta^{(1)}, \omega_\phi^{(1)}$ are the components of vorticity and velocity as a result of the presence of the solid particle a_1 without the second sphere a_2 and $u_r^{(2)},\ u_\theta^{(2)}, \omega_\phi^{(2)}$ are the components of velocity and vorticity of the sphere a_2 without the first sphere a_1 as shown in Fig. 1. Additionally, the subsequent relations link the coordinate systems (r_1, θ_1) and (r_2, θ_2) together as:

$$\left.\begin{aligned} r_1^2 &= r_2^2 + h^2 - 2r_2 h \cos\theta_2\,, \\ r_2^2 &= r_1^2 + h^2 + 2r_1 h \cos\theta_1\,. \end{aligned}\right\} \tag{30}$$

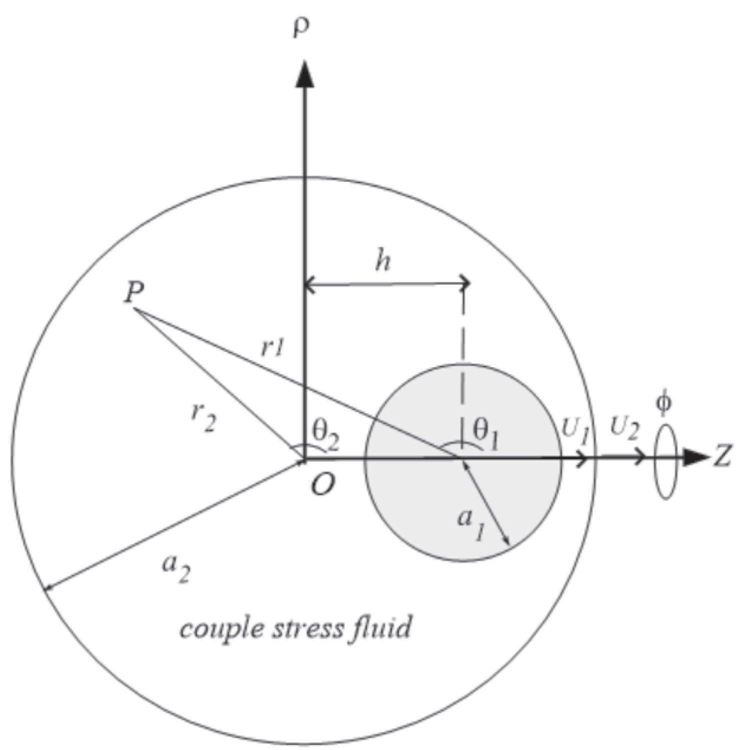

Fig. 1 The geometrical shape of couple stress fluid squeezed two eccentric spheres

As a result, the boundary conditions are linear, allowing for the use of the superposition principle. The following is a representation of the field functions:

$$\begin{bmatrix} u_r(r_1,\theta_1;r_2,\theta_2) \\ u_\theta(r_1,\theta_1;r_2,\theta_2) \\ \tau_{r\theta}(r_1,\theta_1;r_2,\theta_2) \\ m_{r\phi}(r_1,\theta_1;r_2,\theta_2) \end{bmatrix} = \begin{bmatrix} u_r^{(1)}(r_1,\theta_1) \\ u_\theta^{(1)}(r_1,\theta_1) \\ \tau_{r\theta}^{(1)}(r_1,\theta_1) \\ m_{r\phi}^{(1)}(r_1,\theta_1) \end{bmatrix} + \begin{bmatrix} u_r^{(2)}(r_1,\theta_1) \\ u_\theta^{(2)}(r_1,\theta_1) \\ \tau_{r\theta}^{(2)}(r_1,\theta_1) \\ m_{r\phi}^{(2)}(r_1,\theta_1) \end{bmatrix}, \tag{31}$$

The kinematical and dynamical boundary conditions are taken the following forms:

$$u_r\big|_{r_j=a_j} = U_j\cos\theta_j, \quad m_{r\phi}\big|_{r_j=a_j} = 0, \quad j=1,2, \tag{32}$$

$$u_\theta\big|_{r_j=a_j} = \frac{1}{\beta_j}\tau_{r\phi} - U_j\sin\theta_j, \quad m_{r\phi}\big|_{r_j=a_j} = 0, \quad j=1,2. \tag{33}$$

where $\beta_j,\ j=1,2$ are the velocity slippage that has the following properties:

(a) The slip coefficients depend on the nature of the solid and fluid surface.
(b) In the limiting case of $\beta_1 \to 0$, there is a perfect slip and the solid sphere acts like a spherical gas bubble if $\beta_1 \to \infty$, we get the standard no-slip condition.
(c) Also, for $\beta_2 \to 0$ we have the couple stress zero at the boundary which means that the mechanical interactions at the surface are equipollent to a force distribution only. On the other hand, when $\beta_2 \to \infty$ this is equivalent to preventing relative rotation of the fluid element at the surface of the aerosol.

From (32) and use (18), (22), (28) the field functions $u_r,\ u_\theta,\ \tau_{r\theta},\ m_{r\phi}$ are:

$$\begin{aligned} u_r = &-\sum_{n=2}^{\infty}\left[A_n r_1^{-n-1} + B_n r_1^{-n+1} + C_n r_1^{-3/2} K_{n-\frac{1}{2}}(\kappa r_1)\right] P_{n-1}(\zeta_1) \\ &-\sum_{n=2}^{\infty}\left[D_n r_2^{n-2} + E_n r_2^{n} + F_n r_2^{-3/2} I_{n-\frac{1}{2}}(\kappa r_2)\right] P_{n-1}(\zeta_2). \end{aligned} \tag{34}$$

$$\begin{aligned} u_\theta = &\sum_{n=2}^{\infty}\left[(1-n)A_n r_1^{-n-1} + (3-n)B_n r_1^{-n+1} + C_n r_1^{-3/2}\left(n K_{n-\frac{1}{2}}(\kappa r_1) - \kappa r_1 K_{n+\frac{1}{2}}(\kappa r_1)\right)\right]\frac{\Im_n(\zeta_1)}{\sqrt{1-\zeta_1^2}} \\ &+\sum_{n=2}^{\infty}\left[n D_n r_2^{n-2} + (n+2)E_n r_2^{n} + F_n r_2^{-3/2}\left(n I_{n-\frac{1}{2}}(\kappa r_2) + \kappa r_2 I_{n+\frac{1}{2}}(\kappa r_2)\right)\right]\frac{\Im_n(\zeta_2)}{\sqrt{1-\zeta_2^2}}. \end{aligned} \tag{35}$$

$$\begin{aligned} \omega_\phi = &\frac{1}{2}\sum_{n=2}^{\infty}\left[2(3-2n)B_n r_1^{-n} + C_n \kappa^2 r_1^{-1/2} K_{n-\frac{1}{2}}(\kappa r_1)\right]\frac{\Im_n(\zeta_1)}{\sqrt{1-\zeta_1^2}} \\ &+\frac{1}{2}\sum_{n=2}^{\infty}\left[2(2n+1)E_n r_2^{n-1} + F_n \kappa^2 r_2^{-1/2} I_{n-\frac{1}{2}}(\kappa r_2)\right]\frac{\Im_n(\zeta_2)}{\sqrt{1-\zeta_2^2}}. \end{aligned} \tag{36}$$

$$\begin{aligned} m_{r\phi} = 2&\sum_{n=2}^{\infty}\Big[2n(2n-3)(\eta+\eta')B_n r_1^{-n-1} \\ &+C_n \kappa^2 r_1^{-3/2}\left((\eta(n-1)-\eta')K_{n-\frac{1}{2}}(\kappa r_1) - \kappa r_1 \eta K_{n+\frac{1}{2}}(\kappa r_1)\right)\Big]\frac{\Im_n(\zeta_1)}{\sqrt{1-\zeta_1^2}} \\ +2&\sum_{n=2}^{\infty}\Big[2(2n+1)(\eta(n-1)-\eta')E_n r_2^{n-2} \\ &+F_n \kappa^2 r_2^{-3/2}\left((\eta(n-1)-\eta')I_{n-\frac{1}{2}}(\kappa r_2) + \kappa r_2 \eta I_{n+\frac{1}{2}}(\kappa r_2)\right)\Big]\frac{\Im_n(\zeta_2)}{\sqrt{1-\zeta_2^2}}. \end{aligned} \tag{37}$$

$$
\begin{aligned}
\tau_{r\theta} = & \sum_{n=2}^{\infty} \Big[2\mu(n^2-1) A_n r_1^{-n-2} + 2\mu n(n-2) B_n r_1^{-n} \\
& + C_n r_1^{-5/2} \left(\left(\mu(\kappa^2 r_1^2 + 2n^2 - 4n) - \eta\kappa^4 r_1^2 \right) K_{n-\frac{1}{2}}(\kappa r_1) + 2\mu\kappa r_1 K_{n+\frac{1}{2}}(\kappa r_1) \right) \Big] \frac{\Im_n(\zeta_1)}{\sqrt{1-\zeta_1^2}} \\
& + \sum_{n=2}^{\infty} \Big[2\mu n(n-2) D_n r_2^{n-3} + 2\mu(n^2-1) E_n r_2^{n-1} \\
& + F_n r_2^{-5/2} \left(\left(\mu(\kappa^2 r_2^2 + 2n^2 - 4n) - \eta\kappa^4 r_2^2 \right) I_{n-\frac{1}{2}}(\kappa r_2) - 2\mu\kappa r_2 I_{n+\frac{1}{2}}(\kappa r_2) \right) \Big] \frac{\Im_n(\zeta_2)}{\sqrt{1-\zeta_2^2}}
\end{aligned} \tag{38}
$$

The following system is obtained by using Eqs. (34)–(38) and the boundary conditions (32) and (33):

$$
\begin{aligned}
& \sum_{n=2}^{\infty} \left(A_n a_1^{-n-1} + B_n a_1^{-n+1} + C_n a_1^{\frac{-3}{2}} K_{n-\frac{1}{2}}(\ell a_1) \right) P_{n-1}(\zeta_1) \\
& + \sum_{n=2}^{\infty} \left(D_n r_2^{n-2} + E_n r_2^{n} + F_n r_2^{\frac{-3}{2}} I_{n-\frac{1}{2}}(\ell r_2) \right) \Big|_{r_1=a_1} P_{n-1}(\zeta_2) = -U_1\zeta_1,
\end{aligned} \tag{39}
$$

$$
\begin{aligned}
& \sum_{n=2}^{\infty} \left(A_n r_1^{-n-1} + B_n r_1^{-n+1} + C_n r_1^{\frac{-3}{2}} K_{n-\frac{1}{2}}(\ell r_1) \right) \Big|_{r_2=a_2} P_{n-1}(\zeta_1) \\
& + \sum_{n=2}^{\infty} \left(D_n a_2^{n-2} + E_n a_2^{n} + F_n a_2^{\frac{-3}{2}} I_{n-\frac{1}{2}}(\ell a_2) \right) P_{n-1}(\zeta_2) = -U_2\zeta_2,
\end{aligned} \tag{40}
$$

$$
\begin{aligned}
& \sum_{n=2}^{\infty} \frac{G_n(\zeta_1)}{\sqrt{1-\zeta_1^2}} \Big[\left((1-n) - 2\beta_1^{-1} a_1^{-1} \mu(n^2-1) \right) A_n a_1^{-n-1} + \left((3-n) - 2\beta_1^{-1} a_1^{-1} \mu n(n-2) \right) B_n a_1^{-n+1} \\
& + C_n a_1^{\frac{-3}{2}} \left(\left(n - \beta_1^{-1} a_1^{-1} \left(\mu(\kappa^2 a_1^2 + 2n^2 - 4n) - \eta\kappa^4 a_1^2 \right) \right) K_{n-\frac{1}{2}}(\kappa a_1) - \kappa a_1 \left(1 + 2\mu\beta_1^{-1} a_1^{-1} \right) K_{n+\frac{1}{2}}(\kappa a_1) \right) \Big] \\
& + \sum_{n=2}^{\infty} \frac{G_n(\zeta_2)}{\sqrt{1-\zeta_2^2}} \Big[\left(n - 2\beta_1^{-1} r_2^{-1} \mu n(n-2) \right) D_n r_2^{n-2} + \left((n+2) - 2\beta_1^{-1} r_2^{-1} \mu(n^2-1) \right) E_n r_2^{n} \\
& + F_n r_2^{\frac{-3}{2}} \left(\left(n - \beta_1^{-1} r_2^{-1} \left(\mu(\kappa^2 r_2^2 + 2n^2 - 4n) - \eta\kappa^4 r_2^2 \right) \right) I_{n-\frac{1}{2}}(\kappa r_2) + \kappa r_2 \left(1 + 2\beta_1^{-1} r_2^{-1} \mu \right) I_{n+\frac{1}{2}}(\kappa r_2) \right) \Big] \Big|_{r_1=a_1} \\
& = -U_1 \sqrt{1-\zeta_1^2},
\end{aligned} \tag{41}
$$

$$
\begin{aligned}
& \sum_{n=2}^{\infty} \frac{G_n(\zeta_1)}{\sqrt{1-\zeta_1^2}} \Big[\left((1-n) + 2\beta_2^{-1} r_1^{-1} \mu(n^2-1) \right) A_n r_1^{-n-1} + \left((3-n) + 2\beta_2^{-1} r_1^{-1} \mu n(n-2) \right) B_n r_1^{-n+1} \\
& + C_n r_1^{\frac{-3}{2}} \left(\left(n + \beta_2^{-1} r_1^{-1} \left(\mu(\kappa^2 r_1^2 + 2n^2 - 4n) - \eta\kappa^4 r_1^2 \right) \right) K_{n-\frac{1}{2}}(\kappa r_1) - \kappa r_1 \left(1 - 2\mu\beta_2^{-1} r_1^{-1} \right) K_{n+\frac{1}{2}}(\kappa r_1) \right) \Big] \\
& + \sum_{n=2}^{\infty} \frac{G_n(\zeta_2)}{\sqrt{1-\zeta_2^2}} \Big[\left(n + 2\beta_2^{-1} a_2^{-1} \mu n(n-2) \right) D_n a_2^{n-2} + \left((n+2) + 2\beta_2^{-1} a_2^{-1} \mu(n^2-1) \right) E_n a_2^{n} \\
& + F_n a_2^{\frac{-3}{2}} \left(\left(n + \beta_2^{-1} a_2^{-1} \left(\mu(\kappa^2 a_2^2 + 2n^2 - 4n) - \eta\kappa^4 a_2^2 \right) \right) I_{n-\frac{1}{2}}(\kappa a_2) + \kappa a_2 \left(1 - 2\beta_2^{-1} a_2^{-1} \mu \right) I_{n+\frac{1}{2}}(\kappa a_2) \right) \Big] \Big|_{r_2=a_2} \\
& = -U_2 \sqrt{1-\zeta_2^2},
\end{aligned} \tag{42}
$$

$$
\begin{aligned}
& \sum_{n=2}^{\infty} \Big[4n(2n-3)(\eta+\eta') B_n a_1^{-n-1} \\
& + 2C_n \kappa^2 a_1^{\frac{-3}{2}} \left((\eta(n-1) - \eta') K_{n-\frac{1}{2}}(\kappa a_1) - \kappa\, a_1 \eta K_{n+\frac{1}{2}}(\kappa a_1) \right) \Big] \frac{G_n(\zeta_1)}{\sqrt{1-\zeta_1^2}}
\end{aligned}
$$

$$+\sum_{n=2}^{\infty}\Big[4(2n+1)(\eta(n-1)-\eta')E_n r_2^{n-2}$$

$$+2F_n\,\kappa^2 r_2^{\frac{-3}{2}}\left((\eta(n-1)-\eta')I_{n-\frac{1}{2}}(\kappa r_2)+\kappa r_2\eta I_{n+\frac{1}{2}}(\kappa r_2)\right)\Big]\Big|_{r_1=a_1}\frac{G_n(\zeta_2)}{\sqrt{1-\zeta_2^2}}=0\,, \tag{43}$$

$$\sum_{n=2}^{\infty}\Big[4n(2n-3)(\eta+\eta')B_n r_1^{-n-1}$$

$$+2C_n\,\kappa^2 r_1^{\frac{-3}{2}}\left((\eta(n-1)-\eta')K_{n-\frac{1}{2}}(\kappa r_1)-\kappa r_1\eta K_{n+\frac{1}{2}}(\kappa r_1)\right)\Big]\Big|_{r_2=a_2}\frac{G_n(\zeta_1)}{\sqrt{1-\zeta_1^2}}$$

$$+\sum_{n=2}^{\infty}\Big[4(2n+1)(\eta(n-1)-\eta')E_n a_2^{n-2}$$

$$+2F_n\,\kappa^2 a_2^{\frac{-3}{2}}\left((\eta(n-1)-\eta')I_{n-\frac{1}{2}}(\kappa a_2)+\kappa a_2\eta I_{n+\frac{1}{2}}(\kappa a_2)\right)\Big]\frac{G_n(\zeta_2)}{\sqrt{1-\zeta_2^2}}=0\,. \tag{44}$$

The values of the unknown parameters, A_n, B_n, C_n, D_n, E_n and F_n are obtained by solving the resultant system. Numerical checks are made to see if the approximation is converging. As a result, there would be an endless system of unsolvable linear algebraic equations with an unlimited number of unknown coefficients. Using a multiple collocation approach [15–19] helps to prevent this problem. To make the number of unknown coefficients limited, it is necessary to first truncate the infinite series after a finite number of terms. Then, enough locations on the spherical particle's surface have been chosen as collocation sites, where the boundary constraints are strictly enforced to produce the same number of linear equations as coefficients. The drag force can then be calculated by solving these equations. When the particle is close to the cavity, more boundary collocation points are often needed to achieve a given precision.

4 Numerical results

In the results presented in this section, all collocation-based solutions converge to at least five decimal places. We want to quantitatively represent the normalized drag force, F_z/F_∞ acting on the inner solid sphere, a_1 for a range of parameter values found in the equations governing the problem, including slippages $\hat{\beta}_1=\beta_1/\mu a_1^2$, $\hat{\beta}_2=\beta_2/\mu a_1^2$ $\left(0\le\hat{\beta}_1,\hat{\beta}_2<\infty\right)$, couple stress of the first and second kinds $\hat{\eta}=\hat{\eta}/\mu a_1^2$, $\hat{\eta}'=\hat{\eta}'/\mu a_1^2$, $\left(0\le\hat{\eta},\hat{\eta}'<\infty\right)$ the size ratio of the particles $c=a_1/a_2$ $(0.1\le c\le 0.99)$, the velocity ratio U_2/U_1 and the separation parameter $\delta=h/(a_2-a_1)$ $(0.1\le\delta\le 0.99)$. Figures 2, 3, 4, 5, 6, 7, 8 and Tables 1, 2 provide numerical and graphical representations of the effects of the relevant variables on the problem, and Table 3 shows a comparison case with no-slippage as Reference [19].

It is found from Tables 1, 2, and Fig. 2 represent the normalized drag force for slippage cases perfect, partial, and no-slip at certain values of related parameters $\delta=.2$, $\hat{\eta}'=0$. Physically, the slip grows as the interatomic force between solids and liquids rises. The friction coefficient is a more logical method; however, the slip length is the inverse of the slip and may evaluate the capability of the surface to reduce drag. In addition, the dimensionless of the drag force improves with the rise of the size ratio, as $a_1/a_2\to .99$ the curves more near together. For no-slippage, the drag force tends to unity as the classical literature. Moreover, the normalized drag force increases with the increase of the first couple stress parameters.

Figure 3 displays the non-dimensional drag force for various values of slippage parameters and velocity ratio. At the value of the second couple stress parameter from zero to 0.01 the drag force decreases with the increase of slippages, also the drag force decreases with the increase of velocity ratio. On the other hand, Fig. 4 exposes various values of slippages with the corresponding difference in separation parameters that do improvements in the non-dimensional drag force. Figure 5 detects the normalized drag force versus the slippage on the inside sphere for different values of size ratio. The normalized drag force rises quickly for high slippage and improves with the increase of the size ratio. Further, at certain values of the relevant parameters, $U_2/U_1=0.1$, $\hat{\eta}'=0.01$, $c=0.2$, $\hat{\beta}_2=1$, the normalized drag force improves in both situations of the increase

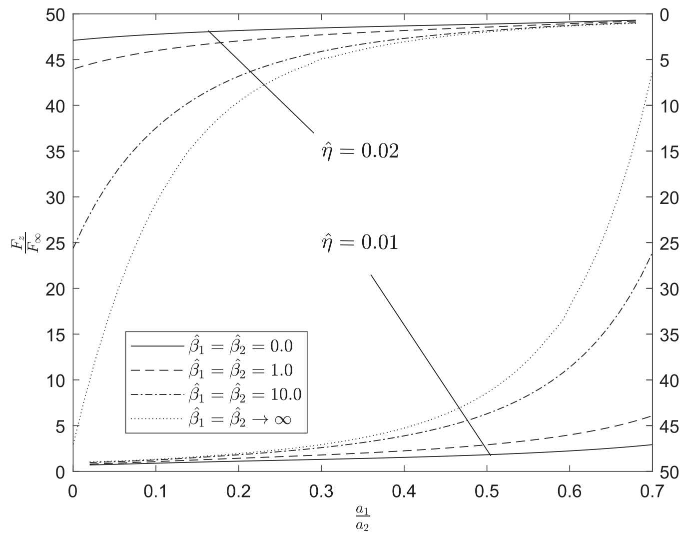

Fig. 2 Non-dimensional drag force on the inside sphere vs the size ratio for fixed outside sphere at $\delta = .2$, $\hat{\eta}' = 0$

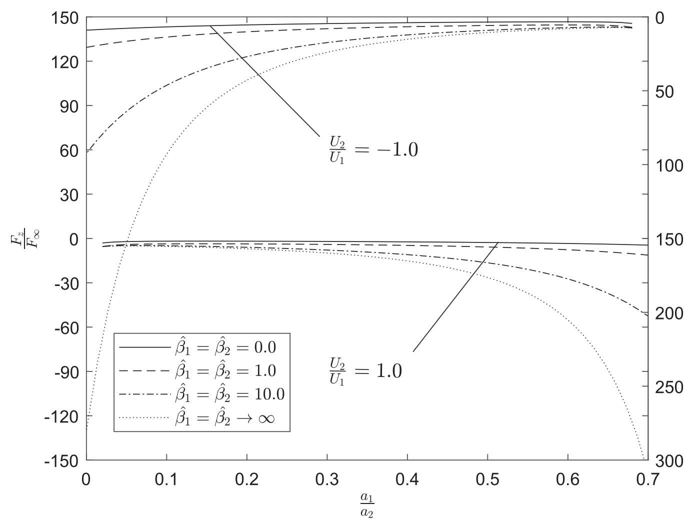

Fig. 3 Non-dimensional drag force on the inside sphere vs the size ratio for at $\delta = 0.01$, $\hat{\eta}' = 0.01$, $\hat{\eta} = 0.01$

of the first couple stress parameter, the separation distance in Fig. 6 and decreases with the increase of the velocity ratio in Fig. 7. Finally, the streamlines for various parameters are sketched when the two spheres move in the same direction with equal speeds.

5 Conclusion

In this work, we investigate the impact of the consistent incompressible axisymmetric coupling stress fluids between the two eccentric spheres on the interfacial slippage on the surfaces of the spheres. The normalized drag force acting on the inner solid sphere is therefore numerically analyzed using the graphs. As a result, a predicted rise in the drag force follows an increase in the couple stress coefficient. Furthermore, it has been demonstrated that an increase in the size ratio and the separation parameter results in a considerable rise in the couple stress fluid flow, which has a major impact on the normalized drag force. In the end, it is found that the slip parameter significantly affects the rise of the normalized drag value. The potential applications in numerous engineering and applied scientific fields, as well as a thorough understanding of hydrodynamics, which provides the theoretical foundation for the design and construction of nanofluidic devices, serve as the driving

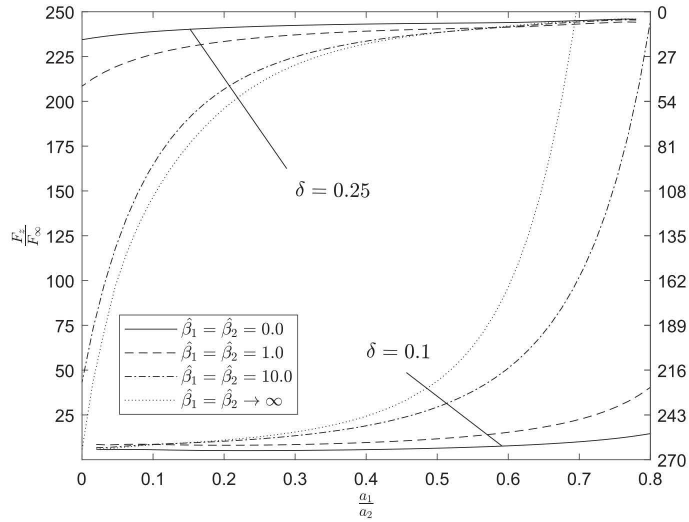

Fig. 4 Non-dimensional drag force on the inside sphere vs the size ratio for at $U_2/U_1 = -1.0$, $\hat{\eta}' = 0.1$, $\hat{\eta} = 0.02$

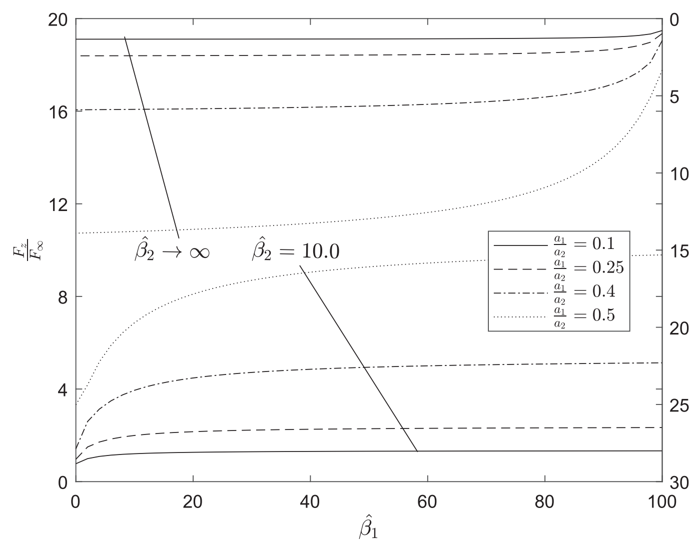

Fig. 5 Non-dimensional drag force on the inside sphere vs the slip for at $U_2/U_1 = -1.0$, $\hat{\eta}' = 0.1$, $\hat{\eta} = 0.02$

forces behind the study of flow slip boundary conditions. Furthermore, understanding the behavior of slip flow in fluid mechanics is crucial for the formation of shale reservoirs. These slip correction factor expressions are not directly applicable to particles of other shapes, as they were all developed based on experimental studies, involving spherical particles only such as [21–26].

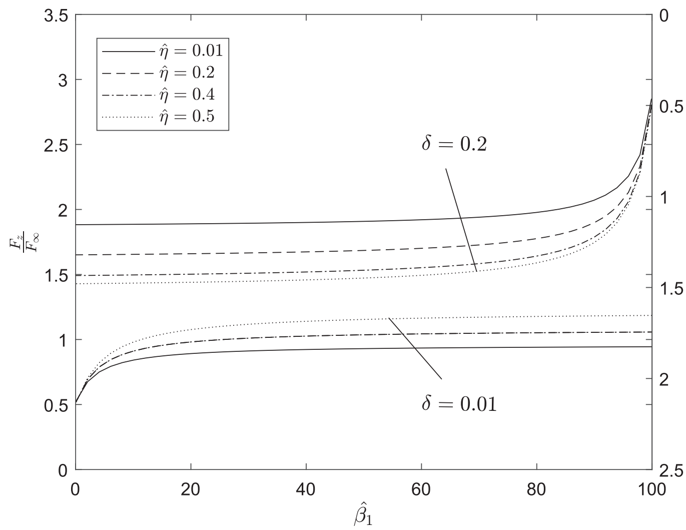

Fig. 6 Non-dimensional drag force on the inside sphere vs the slip for at $U_2/U_1 = 0.1$, $\hat{\eta}' = 0.01$, $c = 0.2$, $\hat{\beta}_2 = 1$

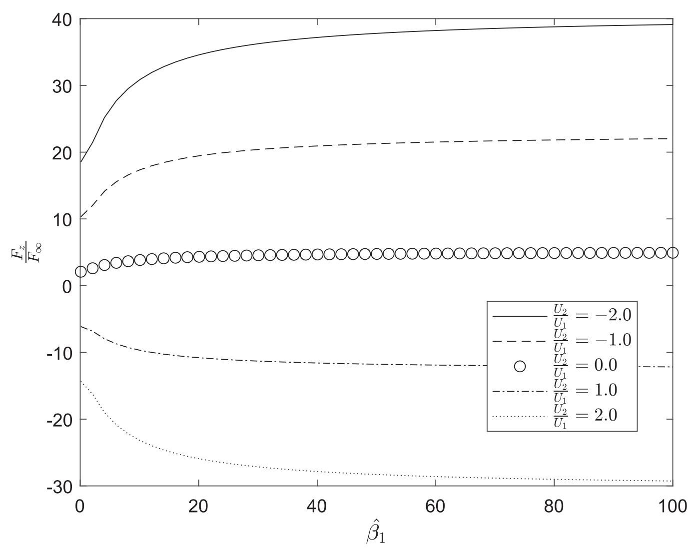

Fig. 7 Non-dimensional drag force on the inside sphere vs the slip at $\delta = 0.01$, $\hat{\eta} = \hat{\eta}' = 0.1$, $c = 0.2$, $\hat{\beta}_2 = 1$, $a_1/a_2 = 0.5$

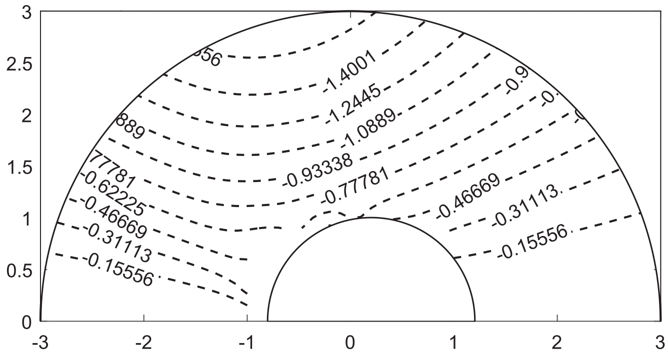

(a) $\hat{\eta} = 0.1, \delta = 0.1$

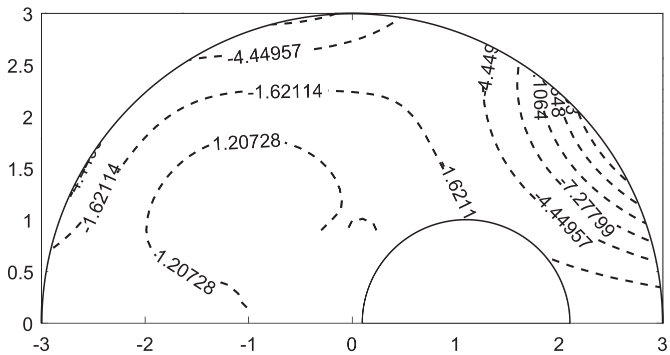

(b) $\hat{\eta} = 0.2, \delta = 0.1$

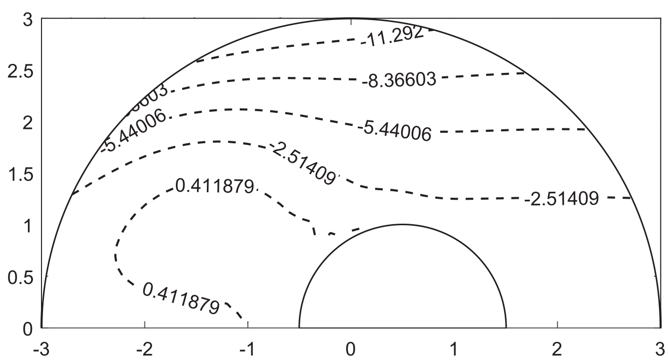

(c) $\hat{\eta} = 0.1, \delta = 0.5$

Fig. 8 The streamlines for various parameters at translation of two spheres with the same velocity in the same direction with second couple parameter 0.1.

Table 1 The non-dimensional drag force acting on the inside sphere with fixed outside sphere at $\hat{\eta}' = 0$

F_z/F_∞					
$\hat{\beta}_1, \hat{\beta}_2$	a_1/a_2	$\hat{\eta} = 0.001$			
		$\delta = 0.01$	$\delta = 0.1$	$\delta = 0.3$	$\delta = 0.5$
0.0	0.1	0.754220	0.850745	0.923402	1.015945
	0.2	0.848063	0.980069	1.237440	1.519690
	0.3	0.968535	1.121742	1.514956	2.046925
	0.4	1.129120	1.302713	1.792638	2.532166
	0.5	1.353922	1.552003	2.131733	3.044978
	0.6	1.691104	1.923254	2.610270	3.705575
	0.7	2.252998	2.539872	3.386060	4.731963
	0.8	3.376408	3.771167	4.920629	6.728266
	0.9	6.743629	7.461513	9.519063	12.689327
	0.99	67.330231	73.837387	91.981392	119.134773
1.0	0.1	0.908186	1.039140	1.069098	1.101668
	0.2	1.082258	1.271032	1.510151	1.625039
	0.3	1.313012	1.539753	1.988076	2.320164
	0.4	1.638710	1.907552	2.541137	3.195199
	0.5	2.134019	2.461544	3.304821	4.341534
	0.6	2.967874	3.390721	4.532855	6.084219
	0.7	4.606352	5.213037	6.892822	9.316928
	0.8	8.827001	9.901094	12.908878	17.436619
	0.9	29.041849	32.319004	41.581177	55.996674
	0.99	2311.570801	2555.071777	3239.885742	4321.527344
10.0	0.1	1.179203	1.273172	1.227720	1.229702
	0.2	1.547653	1.721513	1.769643	1.718155
	0.3	2.136672	2.387121	2.589816	2.513918
	0.4	3.132854	3.501420	3.863806	3.828356
	0.5	4.948851	5.540458	6.148038	6.130208
	0.6	8.630004	9.707602	10.798646	10.746655
	0.7	17.414539	19.745882	21.973087	21.687044
	0.8	45.310505	51.922829	57.620285	56.357807
	0.9	213.139862	246.960709	274.570374	269.995300
	0.99	22827.648438	26424.392578	30003.117188	30354.939453
∞	0.1	1.303745	1.366120	1.285053	1.278389
	0.2	1.779997	1.911866	1.852576	1.755118
	0.3	2.610461	2.805905	2.801343	2.590218
	0.4	4.179204	4.481384	4.408108	4.026001
	0.5	7.479341	8.020477	7.549170	6.606438
	0.6	15.581175	16.757128	14.444007	11.804109
	0.7	40.987663	43.902576	31.450989	23.906670
	0.8	167.482864	164.769760	81.679611	63.195953
	0.9	2414.274902	935.428589	378.217377	326.098022
	0.99	897333.062500	98940.531250	41394.375000	31052.707031

Table 2 The non-dimensional drag force acting on the inside sphere in the opposite direction of the inside sphere at $\hat{\eta}' = 0$

F_z/F_∞					
$\hat{\beta}_1, \hat{\beta}_2$	a_1/a_2	$\hat{\eta} = 0.02$			
		$\delta = 0.01$	$\delta = 0.1$	$\delta = 0.3$	$\delta = 0.5$
0.0	0.1	3.327716	5.587202	5.068946	4.465793
	0.2	3.519153	5.104350	6.622895	6.606525
	0.3	3.943960	5.184700	7.439119	8.953981
	0.4	4.562967	5.629907	8.045003	10.652815
	0.5	5.451842	6.434393	8.911304	12.108415
	0.6	6.790851	7.749751	10.312646	13.593296
	0.7	9.010950	10.007196	12.746773	16.437937
	0.8	13.427116	14.571582	17.743046	21.660469
	0.9	26.694756	28.409849	33.228653	40.403534
	0.99	266.512299	279.486023	317.382751	376.086792
1.0	0.1	5.456466	8.557850	6.801765	5.144554
	0.2	5.842634	8.071379	9.018601	7.293884
	0.3	6.704134	8.454079	10.649095	10.273860
	0.4	8.059993	9.586240	12.245204	13.481561
	0.5	10.197094	11.650284	14.666179	17.099899
	0.6	13.808269	15.311152	18.797148	22.661602
	0.7	20.771584	22.479731	26.767502	32.486546
	0.8	38.128700	40.401932	46.575230	58.196411
	0.9	118.562347	123.371819	138.293442	163.063812
	0.99	8987.805664	9234.860352	10183.305664	12029.856445
10.0	0.1	7.290051	8.582920	5.532883	3.994349
	0.2	9.182245	10.331738	8.216719	5.619449
	0.3	12.420985	13.392817	11.761823	8.426845
	0.4	17.997562	18.925453	16.812393	12.967580
	0.5	28.366117	29.386375	25.827587	20.104612
	0.6	49.785572	51.092793	44.055389	34.560493
	0.7	100.010750	101.918091	86.669533	68.870087
	0.8	241.964783	244.715668	212.188812	174.328842
	0.9	943.919556	945.472412	856.456909	752.522827
	0.99	91103.140625	90646.179688	85045.367188	80273.632813
∞	0.1	7.933994	8.364545	4.974867	3.577955
	0.2	10.508343	10.877122	7.640950	5.051653
	0.3	15.164860	15.183381	11.547580	7.701321
	0.4	24.124905	23.550554	17.429865	11.981995
	0.5	43.885025	41.715073	28.234423	18.988853
	0.6	97.434990	88.324036	49.861652	32.361629
	0.7	293.039307	233.013199	96.560875	63.430847
	0.8	1326.032471	724.638977	228.708099	161.869232
	0.9	8933.410156	3144.214111	1010.574219	781.760254
	0.99	1491927.6250	287864.21875	118200.49219	92670.99219

Table 3 Comparison case with the results of Alsudais et al. [19] at $\hat{\beta}_1, \hat{\beta}_2 \to \infty$ for the non-dimensional drag force acting on the inside sphere in the opposite direction of the inside sphere at $\hat{\eta}' = 0$

$\hat{\eta}$	a_1/a_2	$\delta = 0.001$	$\delta = 0.1$	$\delta = 0.2$	$\delta = 0.3$	$\delta = 0.5$
0.001	0.1	1.335362	1.432209	1.369743	1.328309	1.309569
	0.2	1.811470	1.979858	1.991828	1.901544	1.770427
	0.3	2.655892	2.895778	2.947507	2.861318	2.611798
	0.4	4.261245	4.628690	4.673884	4.489692	4.138749
	0.5	7.654738	8.313003	8.213246	7.626278	6.785348
	0.6	16.030651	17.451588	16.406523	14.153634	11.132277
	0.7	42.475761	45.829765	38.069626	28.758326	19.883070
	0.8	175.043228	168.901245	104.024109	68.236893	52.497513
	0.9	2488.055664	875.846069	428.102112	320.449860	295.231750
0.1	0.1	1.586138	1.763266	1.601907	1.505005	1.437499
	0.2	2.156135	2.397974	2.331649	2.131534	1.896767
	0.3	3.227025	3.531230	3.453674	3.191814	2.795023
	0.4	5.399053	5.815639	5.547643	4.998013	4.456933
	0.5	10.428926	11.026417	9.915304	8.370123	7.101052
	0.6	24.734716	25.056583	19.734396	14.798015	11.468554
	0.7	81.965614	70.264702	42.072887	27.831087	22.825335
	0.8	529.681091	208.381638	98.845871	70.569534	61.778763
	0.9	114918.56231	898.538635	245.619751	132.895599	98.619942

Data availability The data that support the findings of this study are available in the article

Declarations

Conflict of interest The authors have no conflicts to disclose.

References

1. Stokes, V.K., *Couple stresses in fluid*. Physics of Fluids, 1966. **9**: p. 1709-1715.
2. Stokes, V., *Theories of Fluids with Microstructure.* 1984.
3. M, D., S. D, and B. Shanker, *Analytical solutions of couple stress fluid flows with slip boundary conditions.* Alexandria Engineering Journal, 2014. **53**.
4. Gajjela, N., et al., *Entropy Generation Analysis of the MHD Flow of Couple Stress Fluid between Two Concentric Rotating Cylinders with Porous Lining*. Heat Transfer-Asian Research, 2016. 46: p. 316–330.
5. Podila, A., et al., *Couple stress fluid flow due to slow steady oscillations of a permeable sphere.* Nonlinear Engineering, 2020. **9**: p. 352-360.
6. Naz, R., M. Ikram, and M. Asjad, *Analytical solutions of fractional couple stress fluid flow for an engineering problem.* Nonlinear Engineering, 2023. **12**.
7. Thompson, P. and S. Troian, *A General Boundary Condition for Liquid Flow at Solid Surfaces.* Nature, 1997. **389**.
8. Ashmawy, E.A., *Drag on a slip spherical particle moving in a couple stress fluid.* AEJ - Alexandria Engineering Journal, 2016. **55**.
9. Akram, S., et al., *Partial Slip Impact on Double Diffusive Convection Flow of Magneto-Carreau Nanofluid through Inclined Peristaltic Asymmetric Channel*. Mathematical Problems in Engineering, 2021. **2021**: p. 1-14.
10. El-Sapa, S. and A. Almoneef, *The Axisymmetric Migration of an Aerosol Particle Embedded in a Brinkmann Medium of a Couple Stress Fluid with Slip Regime*. European Journal of Pure and Applied Mathematics, 2022. 15: p. 1566–1592.
11. Gluckman , M., R. Pfeffer, and S. Weinbaum, *A new technique for treating multiparticle slow viscous flow: Axisymmetric flow past spheres and spheroids.* Journal of Fluid Mechanics, 1971. **50**: p. 705-740.
12. Chang, Y.C. and H.J. Keh, *Slow motion of a slip spherical particle perpendicular to two plane walls.* Journal of Fluids and Structures, 2006. **22**(5): p. 647-661.
13. Sherief, H., M. Faltas, and S. El-Sapa, *Force on a spherical particle oscillating in a viscous fluid perpendicular to an impermeable planar wall*. Journal of the Brazilian Society of Mechanical Sciences and Engineering, 2019. 41: p. 244 (1–10).
14. Sun, Y., et al., *Prediction of coupled radiative and conductive heat transfer in concentric cylinders with nonlinear anisotropic scattering medium by spectral collocation method.* AIMS Energy, 2021. **9**: p. 581-602.
15. H. Sherief, M. S. Faltas, and S. El-Sapa*, Interaction between two rigid spheres moving in a micropolar fluid with slip surfaces, J. Mol. Liq., 290, 111165 (2019).*
16. T. H. Shehadeh, and E. A. Ashmawy, *"Interaction of two rigid spheres translating collinearly in a couple stress fluid", Eur. J. Mech. B. Fluids, 78, 284–290 (2019).*

17. S. El-Sapa, and M. S. Faltas, *"Mobilities of two spherical particles immersed in a magneto-micropolar fluid", Phys. Fluids, 34 (1), 013104 (2022).*
18. S. El-Sapa, *"Interaction between a non-concentric rigid sphere immersed in a micropolar fluid and a spherical envelope with slip regime", J. Mol. Liq., 351, 118611(2022).*
19. N. S. Alsudais, S. El-Sapa, and E. A. Ashmawy, *"Stokes flow of an incompressible couple stress fluid confined between two eccentric spheres", Eur. J. Mech. B. Fluids, 91, 244–252(2021).*
20. H. Ramkissoon, *Drag in couple stress fluids*, ZAMP 29, 341–346(1978).
21. J. Wedel, M. Štrakl, J. Ravnik, P. Steinmann, M. Hriberšek, *A specific slip length model for the Maxwell slip boundary conditions in the Navier–Stokes solution of flow around a microparticle in the no-slip and slip flow regimes*, Theor. Comput. Fluid Dyn. 36:723–740(2022), https://doi.org/10.1007/s00162-022-00627-w.
22. P. Priyanka, F. Mebarek-Oudina, S. Sahani, S. Arora, Travelling Wave Solution of Fourth Order Reaction Diffusion Equation Using Hybrid Quintic Hermite Splines Collocation Technique, Arabian Journal of Mathematics, 1-39 (2024). https://doi.org/10.1007/s40065-024-00459-y.
23. F. Mebarek-Oudina, I. Chabani, H. Vaidya, A. I. Ismail, Hybrid nanofluid magneto-convective flow and porous media contribution to entropy generation, International Journal of Numerical Methods for Heat & Fluid Flow, 34(2), 809-836 (2024), https://doi.org/10.1108/HFF-06-2023-0326.
24. Priyanka, S. Arora, F. Mebarek-Oudina, S. Sahani, Super convergence analysis of fully discrete Hermite splines to simulate wave behavior of Kuramoto-Shivashinsky equation, Wave Motion, 121, 103187 (2023). https://doi.org/10.1016/j.wavemoti.2023.103187.
25. F. Mebarek-Oudina, Preeti, A. S. Sabu, H. Vaidya, R. W. Lewis, S. Areekara, A. Mathew and A. I. Ismail, Hydromagnetic flow of magnetite-water nano-fluid utilizing adapted Buongiorno model, International Journal of Modern Physics B, 38(1) 2450003 (2024). https://doi.org/10.1142/S0217979224500036.
26. F. Mebarek-Oudina, G. Dharmaiah, K. S. Balamurugan, A. I. Ismail, and H. Saxena, The Role of Quadratic-Linearly Radiating Heat Source with Carreau Nanofluid and Exponential Space-Dependent Past a Cone and a Wedge: A Medical Engineering Application and Renewable Energy. Journal of Computational Biophysics and Chemistry, 22 (8) : 997-1011 (2023), https://doi.org/10.1142/S2737416523420073
27. A. Al-Hanaya, S. El-Sapa, An analysis of slippage effects on a solid sphere enclosed by a non-concentric cavity filled with a couple stress fluids. Scientific Reports 13, 19595 (2023)